Journal of Rock Mechanics and Geotechnical Engineering 14 (2022) 1901–1909

Contents lists available at ScienceDirect

Journal of Rock Mechanics and Geotechnical Engineering

journal homepage: www.jrmge.cn

Full Length Article

Experimental study on the physico-mechanical properties of Tamusu mudstone – A potential host rock for high-level radioactive waste in Inner Mongolia of China

Chen Lu [a,b], Hongdan Yu [a], Honghui Li [c,*], Weizhong Chen [a,**]

[a] State Key Laboratory of Geomechanics and Geotechnical Engineering, Institute of Rock and Soil Mechanics, Chinese Academy of Sciences, Wuhan, 430071, China
[b] University of Chinese Academy of Sciences, Beijing, 100049, China
[c] China Institute for Radiation Protection, Taiyuan, 030006, China

ARTICLE INFO

Article history:
Received 20 July 2021
Received in revised form
30 September 2021
Accepted 21 December 2021
Available online 25 January 2022

Keywords:
Tamusu mudstone
Physico-mechanical properties
High-level radioactive waste (HLW) repository
Disintegration test
Permeability test

ABSTRACT

Tamusu mudstone, located in Bayin Gobi Basin in Inner Mongolia of China, has been selected as a potential host rock for high-level radioactive waste (HLW) disposal in China. A series of tests has been carried out, including X-ray diffraction (XRD) tests, scanning electron microscopy (SEM) tests, disintegration tests, permeability tests and triaxial compression tests, to estimate the physico-mechanical properties of Tamusu mudstone in this work. The mineral composition of Tamusu mudstone was analyzed and it was considered as a stable rock due to its low disintegration rate, i.e. approximately 0.11% after several wet/dry cycles. Based on the results of permeability test, it was found that Tamusu mudstone has a low permeability, with the magnitude of about 10^{-20} m^2. The low permeability makes the mudstone well prevent nuclide migration and diffusion, and might be influenced by temperature. The triaxial tests show that Tamusu mudstone is a stiff mudstone with high compressive strength, which means that the excavation disturbed zone would be smaller compared to other types of mudstone due to construction and operation of HLW repositories. Finally, the properties of Tamusu mudstone were compared with those of Opalinus clay, Callovo-Oxfordian (COx) argillite, and Boom clay to further discuss the possibility of using Tamusu mudstone as a potential nuclear waste disposal medium.

1. Introduction

In recent years, many scientific issues attributed to the widespread use of nuclear energy have received increasing attention. Among them, the disposal of radioactive nuclear waste has received the most attention. Scholars have proposed many ideas for disposing high-level radioactive waste (HLW), such as ice cover, ocean disposal, seabed disposal, outer space disposal, and deep geological disposal. At present, the most acceptable way is the deep geological disposal. Clayey rocks due to their favorable advantages, such as low permeability, strong ion exchange, strong adsorption, and fracture self-sealing, have been selected as a potential surrounding rock in HLW repositories in many countries.

Switzerland built an underground rock laboratory called Mont Terri in the Canton of Jura. At this laboratory, many field and laboratory tests have been performed to study the physical properties of Opalinus clay, including physico-mechanical characteristics such as the mineral composition, permeability characteristics, excavation disturbed zone (EDZ), and thermo-hydro-mechanical (THM) characteristics (Thury and Bossart, 1999; Martin and Lanyon, 2003; Bossart et al., 2004, 2017; Croise et al., 2004; Wersin et al., 2004; Kull et al., 2007; Amann et al., 2011, 2012).

The French National Radioactive Waste Management Agency (Andra) has built an underground HLW laboratory in Bure, Meuse/Haute Marne Province, to study the feasibility of Callovo-Oxfordian (COx) argillite to be the surrounding rock of the repository. Many tests have been conducted at this laboratory. The field tests at this site have mainly investigated the evolution of the EDZ permeability characteristics, hydro-mechanical (HM) and THM properties, and long-term creep properties of COx argillite (Andra, 2005; de la Vaissière et al., 2015; Armand et al., 2017a). Some scholars have studied the HM properties of COx argillite through laboratory tests.

* Corresponding author.
** Corresponding author.
E-mail addresses: yz202lhh@163.com (H. Li), wzchen@whrsm.ac.cn (W. Chen).
Peer review under responsibility of Institute of Rock and Soil Mechanics, Chinese Academy of Sciences.

https://doi.org/10.1016/j.jrmge.2021.12.016

For example, Homand et al. (2004) used the pulse method to measure the permeability of saturated COx argillite samples and improved the equipment and methods to measure the permeability of unsaturated rock samples. Zhang (2016) studied the relationship between permeability and volumetric strain of COx argillite, and his results showed that the permeability first decreased and subsequently increased with increasing volumetric strain. Armand et al. (2017b) systematically studied the HM characteristics of COx argillite. Zhang (2018) summarized the THM properties of COx argillite in detail and improved the understanding of COx argillite THM properties.

Belgian Nuclear Research Centre (SCK·CEN) established the HADES underground laboratory at a preselected site in the Boom clay layer within the Mol-Dessel region and invited experts from many countries to study the physico-mechanical properties of Boom clay under multifield coupling. De Bruyn and Thimus (1996) performed triaxial tests at high temperatures and found that the strength and elastic modulus of Boom clay were dependent on the temperature. Delage et al. (2000) studied the permeability coefficient of Boom clay at different temperatures. Their results showed that the hydraulic conductivity of Boom clay increased at higher temperature. Based on field tests at the HADES underground research laboratory, the evolution of the permeability within the EDZ of the surrounding rock of Boom clay was studied (Bastiaens et al., 2007; Van Marcke and Bastiaens, 2010). These studies showed that from 2004 to 2005, the hydraulic conductivity of the surrounding rock in the connecting gallery in the horizontal and vertical directions tended to decrease, and the difference of the hydraulic conductivity in these two directions gradually decreased.

During the past decade, our research team focused on studying the THM properties of Boom clay (Yu et al., 2012, 2014, 2015, 2018; Ma et al., 2016). For example, Ma et al. (2016) studied the evolution law of the permeability of Boom clay in both horizontal and vertical directions under complicated conditions, i.e. different temperatures and loading paths. Yu et al. (2018) performed triaxial tests under THM coupling, and their results showed that the shear strength, elastic modulus and cohesion of Boom clay decreased when temperature increased. However, the effect of temperature on the friction angle is not substantial.

In China, much more effort has been made to granite in Beishan, Gansu Province, for HLW underground disposal during the past decades. Indeed, the study on HLW disposal in mudstone has just begun. A few researches have been performed related to the HLW disposal in mudstones, such as regional preselection, section preselection and site evaluation. According to the natural, social and economic conditions, Tamusu mudstone in the Bayin Gobi Basin, which is located in Inner Mongolia of China, has been selected as a candidate host rock of the HLW repository (Du et al., 2017; He et al., 2019; Xiang et al., 2020). On the basis of previous studies, this paper presents basic information on physico-mechanical properties of Tamusu mudstone and gives a comparison with other clayey rocks mentioned above. The core samples used in this paper were drilled from the Yingejing Sub-basin, with the core hole number of TZK-2. The storage method and properties of the cores were shown in Xiang et al. (2020).

2. Analyses of mineral compositions of Tamusu mudstone

2.1. Methodology

Representative rock blocks were selected for analyzing the mineral compositions of Tamusu mudstone using scanning electron microscopy (SEM) and X-ray diffraction (XRD). The rock samples were ground into powder and passed through a 40 μm square hole sieve. Then the screened powder was dried at 40 °C for 24 h. Finally, the powder was sealed and stored. In order to obtain the clay mineral content, the clay fractions (<2 μm) of the samples were investigated using oriented mounts in the air-dried state after ethylene glycol solvation and after heating at 495 °C.

A Bruker D8 ADVANCE X-ray diffractometer was adopted to analyze the mineral compositions of Tamusu mudstone at room temperature. The diffractometer is operated by CuKα radiation with the tube current of 40 mA and the tube voltage of 40 kV. The scanning range of the diffractometer is 5°–50° with a step size of 0.02°, and the counting time is 0.3 s.

A FEI Quanta 250 scanning electron microscope with INCA X-MAX50 EDX detector produced by the FEI Company (USA) was used to analyze rock samples. Since the rock sample was not conductive, gold spraying treatment was carried out. The SEM tests were conducted under an accelerating voltage of 20 kV and a working distance of 15.4 mm.

2.2. Analysis of XRD and SEM results

Different mineral compositions of Tamusu mudstone can be distinguished from the XRD traces according to the value and angle of the characteristic peak. Results of the mineral composition analysis are shown in Table 1 and Fig. 1, and SEM images of the samples are shown in Fig. 2.

The mineral composition analysis shows that the percentages of dolomite, plagioclase, and quartz, which have high strength (Wang et al., 2017), are relatively high, occupying 77% of the sample. Combined with XRD results, we can find quartz, dolomite, plagioclase and clay minerals in Fig. 2.

The clay minerals occupy around 13% in the Tamusu mudstone, which mainly consists of illite and illite/smectite interstratified minerals. These clay minerals have strong ion exchange characteristics and adsorption capacity, which can effectively prevent the migration of radionuclides (He et al., 2019; Zhang et al., 2020). Furthermore, the Tamusu mudstone contains 1% of analcime which may enhance the radionuclide adsorption properties (Xiang et al., 2020). It will benefit for absorption of nuclide for high-level radioactive waste underground disposal. Moreover, Fe^{2+} in pyrite, which accounts for 5% of the total sample, can reduce the high valence radionuclides and reduce their migration and diffusion capacity. S^- in pyrite can consume H_2O_2 produced by the radiation to groundwater, which is beneficial to maintain the reduction atmosphere of the repository (Chen et al., 2010).

The massive particles of Tamusu mudstone are closely arranged, and the anisotropy is observed in the microstructure (see Fig. 2). There are many massive grain crystal minerals in the sample, with different sizes and irregular shapes. The sample micrographs show that the largest grain crystal is approximately 7 μm, whereas the smallest one is approximately 0.1 μm. Pores are observed in the micrographs among the clay mineral particles or between clay and non-clay mineral particles, some of which are filled with solid particles. Microcracks can be observed in the micrographs, primarily in the intergranular and intragranular regions. Most of these microcracks are irregular in shape, with good extensibility and different lengths.

SEM images reveal that the microstructure of Tamusu mudstone is anisotropic. Former researches (Dehandschutter et al., 2004,

Table 1
Mineral composition (%) of Tamusu mudstone.

Quartz	Dolomite	Pyrite	Clay minerals		Analcime	Plagioclase	Others
			Illite	Illite/smectite			
20	36	5	5	8	1	21	4

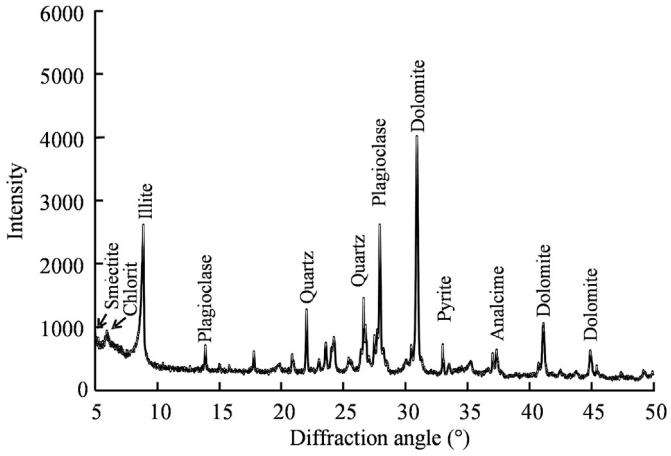

Fig. 1. XRD traces of representative rock blocks.

2005) on Boom clay samples taken at a depth of several metres in the sidewall of a tunnel also revealed obvious differences in the microscopic junction between the perpendicular and parallel directions to the bedding plane. The anisotropy is an important factor that affects the mechanical properties of clayey rock and plays an important role in THM coupling. The anisotropy of the mechanical properties of Tamusu mudstone must be in-depth investigated in future studies.

3. Disintegration tests on Tamusu mudstone

3.1. Test preparation

Six cylindrical samples, each of which has a diameter of 25 mm and a length of 50 mm, were prepared and numbered as BJ-1 to BJ-6. The basic details of the disintegration test samples are shown in Table 2. A photograph of the sample BJ-6 is shown in Fig. 3.

3.2. Test procedure

The disintegration tests were performed according to the following procedure:

(1) The samples were placed in an oven at 105 °C for 24 h, during which the samples were continuously dried.

Table 2
Basic characteristics of the disintegration test samples.

Sample No.	Initial weight (g)	Water content (%)	Density (kg/m^3)
BJ-1	60.7	2.31	2471.905
BJ-2	62.13	1.95	2531.165
BJ-3	61.4	1.78	2529.904
BJ-4	61.59	1.55	2519.979
BJ-5	56.19	2.08	2501.28
BJ-6	57.95	3.4	2501.083

(2) The samples were moved out of the oven and cooled to room temperature, after which they were ground, sieved and weighed.
(3) The samples were placed into distilled water and soaked for 24 h.
(4) Steps (1)–(3) were repeated 5 times in total.

The electronic scale in this test had a capacity of 1000 g and an accuracy of 0.01 g. The temperature of the test environment was controlled at 25 °C. Rubber gloves were worn when contacting the sample during weighing, and the measurements were conducted immediately after the room temperature was reached to avoid the dried samples absorbing moisture from the air and minimize the temperature changing effects.

3.3. Test results

The results obtained from the disintegration tests are shown in Table 3. After 5 wet/dry cycles, few disintegrated particles and blocks were found in the samples, and the integrities were maintained. According to a visual inspection, Tamusu mudstones did not collapse or sustain any visible cracks or defects. The samples at the end of the test seemed approximately identical to their state before testing. The disintegration rate of Tamusu mudstone can be defined as follows (Wu et al., 2010):

$$D_m = m_1/m_2 \tag{1}$$

where D_m is the disintegration rate, m_1 is the mass of the rock sample during testing, and m_2 is the mass of the first weighting. The results of the sample disintegration rates are shown in Fig. 4.

As the sample is small, the test results inevitably have a certain degree of discreteness. The average of the test results is shown by the dotted line in Fig. 4. The disintegration rate of the sample increases when the number of wet/dry cycles increases. The average

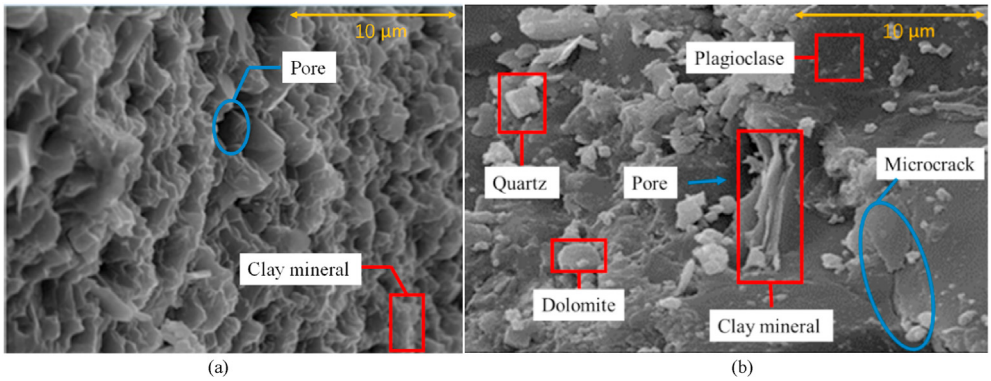

(a) (b)

Fig. 2. SEM images of Tamusu mudstone: (a) Perpendicular and (b) parallel to the bedding plane.

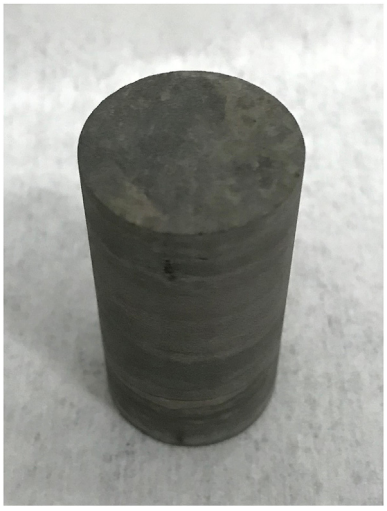

Fig. 3. Photograph of the sample BJ-6.

Table 3
Measurements from the disintegration tests.

Sample No.	First weighing (g)	Second weighing (g)	Third weighing (g)	Fourth weighing (g)	Fifth weighing (g)	Sixth weighing (g)
BJ-1	60.38	60.38	60.34	60.32	60.31	60.29
BJ-2	61.83	61.82	61.8	61.77	61.75	61.73
BJ-3	61.08	61.08	61.07	61.07	61.07	61.05
BJ-4	61.23	61.21	61.19	61.17	61.17	61.16
BJ-5	55.85	55.85	55.84	55.84	55.84	55.83
BJ-6	57.45	57.45	57.42	57.41	57.36	57.35

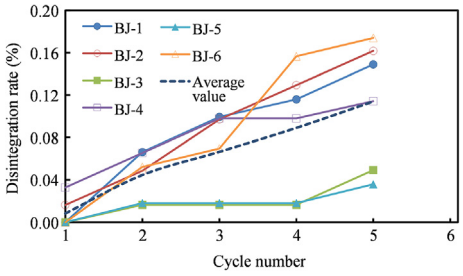

Fig. 4. Disintegration test results.

disintegration rate is approximately linear, especially after the second wet/dry cycle.

The disintegration characteristics of Tamusu mudstone are very weak. The disintegration rates of samples BJ-1 to BJ-6 were 0.15%, 0.16%, 0.05%, 0.11%, 0.04% and 0.17%, respectively, with an average value of 0.11% after 5 wet/dry cycles. The results of the mineral composition analysis in Section 2 revealed that the clay mineral content was 13%, including 8% illite/smectite. This composition contributes to Tamusu mudstone expansion (Helmy, 1998; Hensen and Smit, 2002) and disintegration (Morrow et al., 2000; Kong et al., 2018; Yang et al., 2019) when the mudstone comes in contact with water.

The physical properties of Tamusu mudstone remain stable after water exposure, which makes it difficult to disintegrate. Therefore, when a saturated rock sample is required before testing, it can be saturated in a vacuum saturation cylinder, which can improve the saturation efficiency.

4. TH coupled properties of Tamusu mudstone

4.1. Test preparation

For the permeability measurement, two cylindrical Tamusu mudstone samples, each with a diameter of 38 mm and a height of 20 mm, were prepared and labelled as TMS01 and TMS02 (Fig. 5), respectively. The samples were collected in the direction parallel to the bedding plane and thus the measured permeability of the mudstone was normal to the bedding plane. Following the suggestions in the literature (Boulin et al., 2012), the hydraulic conductivity and intrinsic permeability of Tamusu mudstone were measured by the steady-state method. According to the in situ field test results provided by Du et al. (2017) and Huang (2018), if the geological disposal repository of nuclear waste is built at a depth of 500 m underground, both the horizontal and vertical stresses will be approximately 10 MPa, and the pore water pressure will be 4–5 MPa. Therefore, for the permeability test, the hydrostatic pressure is 10 MPa ($\sigma_1 = \sigma_2 = \sigma_3 = 10$ MPa) and the backpressure is 4 MPa ($\Delta p = 4$ MPa). The radioactive nuclide in HLW will release heat due to decay during geological disposal, which results in a substantial increase in the temperature of the surrounding rock of the disposal repository (Weetjens and Sillen, 2005). Therefore, in the permeability test, the temperature change is 20 °C→40 °C→60 °C→80 °C→60 °C→40 °C→20 °C, and the heating/cooling rate is 1 °C/h. The thermo-mechanical loading path is shown in Fig. 6.

4.2. Test results

The permeability test results are shown in Fig. 7. The hydraulic conductivity of Tamusu mudstone varies from 1×10^{-13} m/s to 1×10^{-12} m/s with respect to changes in temperature, and the intrinsic permeability is very low, in the range of 1×10^{-20}–4×10^{-20} m^2. According to the SEM analysis in Section 2, Tamusu mudstone particles are closely arranged, and there are pores among the clay mineral particles or between clay and non-clay mineral particles. Some pores are filled with crystallized mineral particles, which may slow or even stop the flow of pore water, and thus lead to the low permeability of Tamusu mudstone.

The variations in hydraulic conductivity and intrinsic permeability of Tamusu mudstone have the same trend as the temperature varies. When the temperature increases from 20 °C to 80 °C, the hydraulic conductivity of Tamusu mudstone increases from 1.05×10^{-13} m/s to 1.01×10^{-12} m/s (a 10-fold increase), and the intrinsic permeability increases from 1.07×10^{-20} m^2 to 3.78×10^{-20} m^2 (a 3.5-fold increase). These results indicate that the increase of the hydraulic conductivity during heating is mainly due to the decreases of the pore water density and dynamic viscosity coefficient. On a macroscopic level, the Tamusu mudstone sample may exhibit volumetric expansion. Whereas on a microscopic level, the sample may exhibit pore expansion and microfracture system propagation or coalescence.

The changes in hydraulic conductivity and intrinsic permeability of Tamusu mudstone during cooling are smaller than those during heating. Thus, at the same temperature, the hydraulic conductivity and intrinsic permeability during cooling are larger than the values during heating. When the temperature returns to 20 °C, the hydraulic conductivity and intrinsic permeability increase by a factor of 2.3, which shows that the heating stage may cause Tamusu mudstone to exhibit thermal expansion. This thermal expansion results in irreversible changes in the microstructure of Tamusu mudstone, resulting in the permeability that cannot be restored to its original state in the cooling stage.

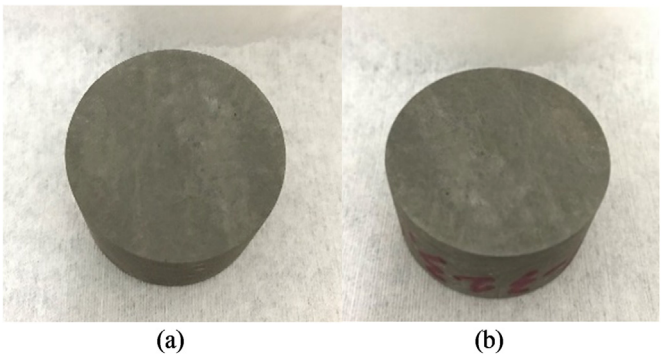

Fig. 5. Photograph of Tamusu mudstone samples: (a) TMS01 and (b) TMS02.

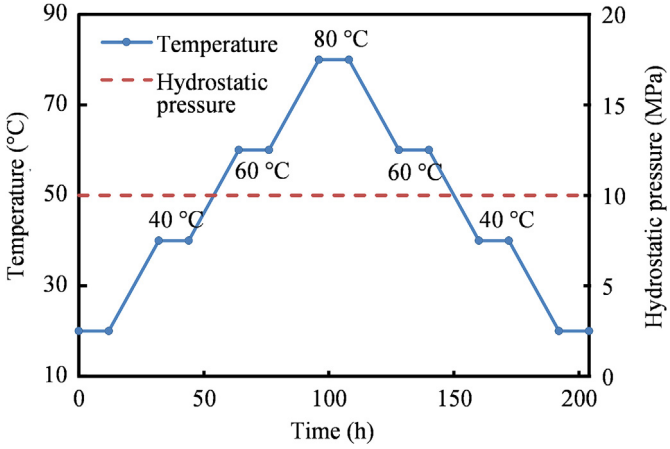

Fig. 6. Thermo-mechanical loading path.

5. Mechanical properties of Tamusu mudstone

5.1. Test preparation

Cylindrical samples with a diameter of 50 mm and a length of 100 mm were used for the conventional triaxial compression test (the confining pressure was 5 MPa, 10 MPa and 15 MPa; and the water pressure was 5 MPa). A photograph of the test sample is shown in Fig. 8. The environmental temperature during testing was controlled at 22 °C. During the test, the sample was subjected to a constant strain rate of 10^{-6} s^{-1} and could be regarded as quasi-static (Bieniawski and Bernede, 1979). The loading axis was perpendicular to the bedding plane.

5.2. Test results

The results of the conventional triaxial compression test are shown in Fig. 9. It can be observed that the whole process can be divided into three stages: compaction stage, elastic stage, and plastic strengthening stage. In the compaction stage, the stress slowly increases, and the strain rapidly increases. Meanwhile, the volumetric strain increases in this stage, and the sample is compacted. Then, the sample enters the elastic stage, where the stress–strain relationship is linear, the volumetric strain continues to increase, and the sample continues to be compressed. When the strain increases and the sample comes into the plastic strengthening stage, wherein the stress nonlinearly increases with respect to the strain. The volumetric strain first increases and subsequently decreases, and the sample begins to expand. Finally, the stress reaches the peak value, after which the sample is destroyed.

SEM images of the intact Tamusu mudstone (Fig. 2) show that there are microcracks and pores in the intergranular regions of the sample. Thus, in the early stage of loading, the fractures and pores in the sample are closed, which are the characteristic of the compaction stage. Then, due to the friction between closed fractures, no relative sliding occurs between the microfractures, which is the characteristic of the elastic stage. In the plastic strengthening stage, plastic deformation and volumetric expansion occur in response to the initiation and development of the microfracture system and slip between fracture surfaces. Finally, the microcracks expand and connect to form macroscopic cracks, and then the sample fails.

The confining pressure also affects the mechanical properties of Tamusu mudstone. A higher confining pressure corresponds to a greater ultimate strain. The ductility increases from 6.3×10^{-3} at 5 MPa to 7.7×10^{-3} at 15 MPa. With the increase in confining pressure from 5 MPa to 15 MPa, the peak strength of Tamusu mudstone tends to increase from 24.1 MPa to 68.4 MPa. Moreover, at the confining pressure of 15 MPa, strain softening occurs after

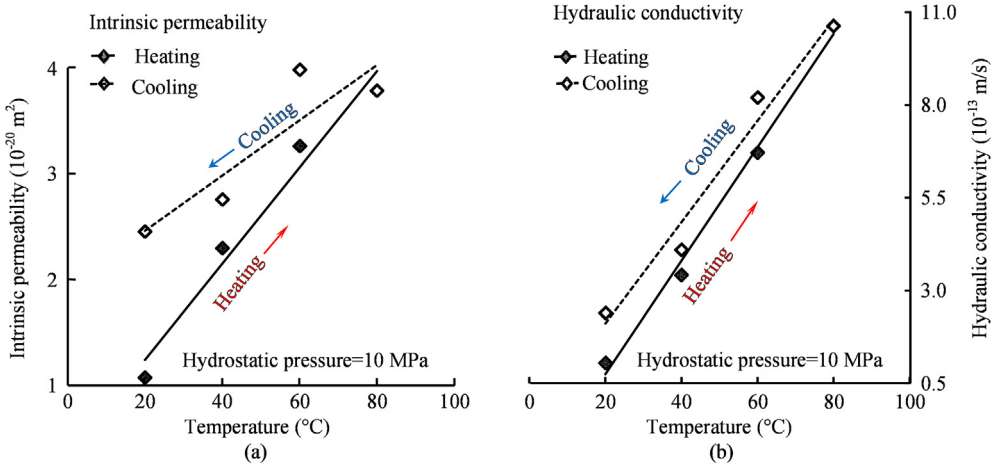

Fig. 7. Permeability test results.

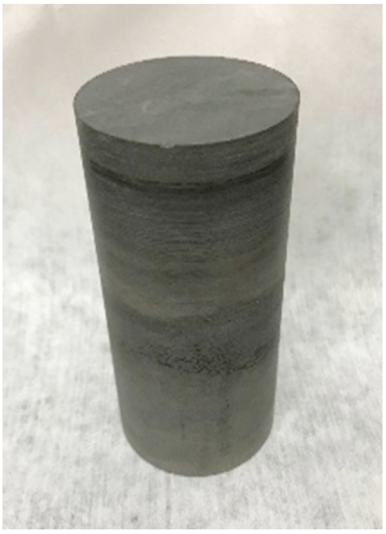

Fig. 8. Photograph of sample for the conventional triaxial compression test.

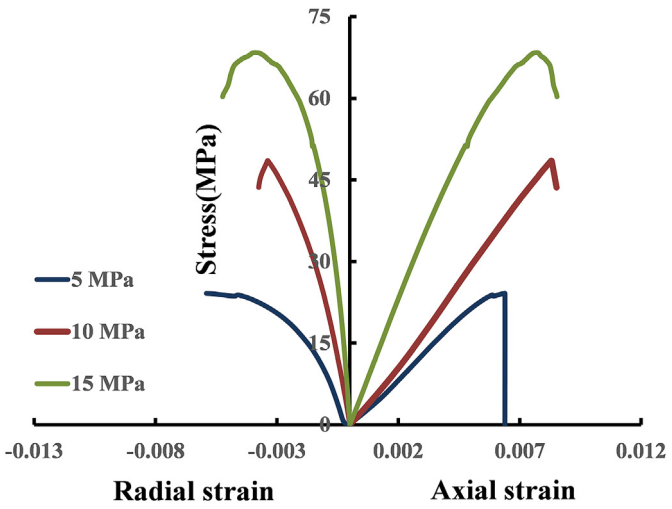

Fig. 9. Stress–strain response from the conventional triaxial compression test.

the peak strength is reached, which is different from the brittle failure of other samples.

5.3. Transversely isotropic elastoplastic constitutive model

The Tamusu region is composed of a continuous layer of thick lacustrine mudstone and samples from this region contain typical laminar structures (Xiang et al., 2020). According to the layered characteristics of Tamusu mudstone, a transversely isotropic elastoplastic constitutive model is proposed for describing its stress–strain behavior using the approach and framework proposed by Yu et al. (2014) and Ma et al. (2018).

The effective stress tensor is $\boldsymbol{\sigma} = \boldsymbol{\sigma}' - \delta \boldsymbol{u}$, where $\boldsymbol{\sigma}'$ is the total stress tensor, δ is the Kronecker delta, and $\boldsymbol{u}$ is the pore water pressure. The effective stress tensor $\boldsymbol{\sigma}$ is linked with the strain tensor $\boldsymbol{\varepsilon}$ through the general Hooke law (Hong et al., 2014):

$$\{\mathrm{d}\boldsymbol{\sigma}\} = [C]_{\mathrm{ep}}\{\mathrm{d}\boldsymbol{\varepsilon}\} \tag{2}$$

where $[C]_{\mathrm{ep}}$ is the elastoplastic tangential stiffness matrix, and it can be expressed as follows:

$$[C]_{\mathrm{ep}} = [C] - \frac{[C]\left\{\frac{\partial G_{\mathrm{s}}}{\partial \boldsymbol{\sigma}}\right\}\left\{\frac{\partial F_{\mathrm{s}}}{\partial \boldsymbol{\sigma}}\right\}^{\mathrm{T}}[C]}{A + \left\{\frac{\partial F_{\mathrm{s}}}{\partial \boldsymbol{\sigma}}\right\}^{\mathrm{T}}[C]\left\{\frac{\partial G_{\mathrm{s}}}{\partial \boldsymbol{\sigma}}\right\}} \tag{3}$$

where F_{s} is the plastic yield surface; G_{s} is the plastic potential function; and $[C]$ is the elastic stiffness matrix, which is given as follows (Yu et al., 2014):

$$[C]^{-1} = \begin{bmatrix} \frac{1}{E_{\mathrm{h}}} & \frac{-\nu_{\mathrm{hh}}}{E_{\mathrm{h}}} & \frac{-\nu_{\mathrm{vh}}}{E_{\mathrm{v}}} & 0 & 0 & 0 \\ \frac{-\nu_{\mathrm{hh}}}{E_{\mathrm{h}}} & \frac{1}{E_{\mathrm{h}}} & \frac{-\nu_{\mathrm{vh}}}{E_{\mathrm{v}}} & 0 & 0 & 0 \\ \frac{-\nu_{\mathrm{vh}}}{E_{\mathrm{h}}} & \frac{-\nu_{\mathrm{vh}}}{E_{\mathrm{h}}} & \frac{1}{E_{\mathrm{v}}} & 0 & 0 & 0 \\ 0 & 0 & 0 & \frac{2(1+\nu_{\mathrm{hh}})}{E_{\mathrm{h}}} & 0 & 0 \\ 0 & 0 & 0 & 0 & \frac{1}{G_{\mathrm{vh}}} & 0 \\ 0 & 0 & 0 & 0 & 0 & \frac{1}{G_{\mathrm{vh}}} \end{bmatrix} \tag{4}$$

where E_{v} and E_{h} are the elastic moduli in the directions perpendicular and parallel to the bedding plane, respectively; ν_{hh} and ν_{vh} and are the Poisson's ratios; and G_{vh} is the shear modulus.

The plastic hardening modulus A in Eq. (3) is calculated as follows:

$$A = -\frac{\partial F_{\mathrm{s}}}{\partial h_{\mathrm{p}}}\left\{\frac{\partial h_{\mathrm{p}}}{\partial \boldsymbol{\varepsilon}^{\mathrm{p}}}\right\}^{\mathrm{T}}\left\{\frac{\partial G_{\mathrm{s}}}{\partial \boldsymbol{\sigma}}\right\} \tag{5}$$

where ε^{p} is the plastic strain tensor; and h_{p} is the plastic damage parameter, which is introduced in a hyperbolic form (Ma et al., 2018):

$$h_{\mathrm{p}} = h_{\mathrm{p0}} + \frac{b_{\mathrm{p}}(1-h_{\mathrm{p0}})\xi_{\mathrm{p}}}{(1-h_{\mathrm{p0}}) + b_{\mathrm{p}}\xi_{\mathrm{p}}} \tag{6}$$

where h_{p0} and b_{p} are the model parameters; and ξ_{p} is the equivalent plastic deviatoric strain, which is given as

$$\left.\begin{aligned} \mathrm{d}\xi_{\mathrm{p}} &= \sqrt{\frac{2}{3}\mathrm{d}\boldsymbol{e}_{\mathrm{p}}:\mathrm{d}\boldsymbol{e}_{\mathrm{p}}} \\ \mathrm{d}\boldsymbol{e}_{\mathrm{p}} &= \mathrm{d}\boldsymbol{\varepsilon}_{\mathrm{p}} - \frac{1}{3}\mathrm{tr}(\mathrm{d}\boldsymbol{\varepsilon}_{\mathrm{p}})\delta \end{aligned}\right\} \tag{7}$$

where $\boldsymbol{e}_{\mathrm{p}}$ is the plastic deviatoric strain.

The relationship between the cohesion c_{p} and the plastic damage parameter h_{p} is assumed as follows:

$$c_{\mathrm{p}} = h_{\mathrm{p}}c_0 \tag{8}$$

where c_0 is the initial cohesion.

The relationship between the friction angle φ and the plastic damage parameter h_{p} is assumed as follows:

$$\varphi = \arctan(h_{\mathrm{p}}\tan\varphi_0) \tag{9}$$

where φ_0 is the initial friction angle.

The plastic yield surface F_{s} is consistent with the Drucker–Prager model:

$$F_s = q - \alpha p - k = 0 \tag{10}$$

where α and k are the slope and intercept on the q-p plane of the shear failure surface, respectively, which are represented as

$$p = \frac{1}{3}\mathrm{tr}(\boldsymbol{\sigma}) \tag{11}$$

$$q = \left(\frac{3}{2}\boldsymbol{s} : \boldsymbol{s}\right)^{\frac{1}{2}} \tag{12}$$

$$\boldsymbol{s} = \boldsymbol{\sigma} - \frac{1}{3}p\delta \tag{13}$$

where $\boldsymbol{s}$ is the deviatoric stress tensor.

The expressions of α and k are related to the cohesion and friction angle:

$$\alpha = \frac{\sin\varphi}{5(3 - \sin\varphi)} \tag{14}$$

$$k = 10c_p\frac{\cos\varphi}{3 - \sin\varphi} \tag{15}$$

The plastic potential surface function G_s is taken as follows:

$$G_s = F_s \tag{16}$$

The presence of confining pressure will affect the elastic modulus in the directions parallel and perpendicular to the bedding plane, i.e. E_h and E_v are related to the confining pressure and calculated from the test results, as shown in Table 4. The remaining parameters are listed in Table 5.

The simulation results match well with the experimental results by calling the UMAT subroutine in ABAQUS (Fig. 10). Given the limited experimental data, the transversely isotropic elastoplastic constitutive model of Tamusu mudstone requires more in-depth study.

6. Discussion

To further discuss the possibility of using Tamusu mudstone as a host rock for the geological disposal of HLW, the basic physico-mechanical properties of Tamusu mudstone are compared with those of Opalinus clay in Switzerland, COx argillite in France and Boom clay in Belgium, as shown in Table 6.

Compared to the other three types of clayey rocks, Tamusu mudstone has higher density, elastic modulus in the direction perpendicular to the bedding plane and compressive strength, which are 2.55 g/cm^3, 4 GPa, and 24.1 MPa, respectively. The higher strength of Tamusu mudstone may ensure its stability during excavation. Thus, if using this material as the surrounding rock for a HLW repository, the cost of the project may be reduced, and the construction efficiency may be improved.

The water content of Boom clay is relatively high. Bastiaens et al. (2006) and Yu et al. (2015) showed that Boom clay has strong HM characteristics, and similar properties have been found in the tests of Opalinus clay and COx argillite under HM coupling (Armand et al., 2017b). However, Tamusu mudstone has the lowest water content (approximately 2.2%), which indicates that the HM characteristics of Tamusu mudstone may not be obvious. Moreover, although the intact Tamusu mudstone sample displays lowest permeability of 1×10^{-20} m^2 compared with other candidate host clayey rocks, the SEM image shows that it contains many pores and microfractures, which indicates that the connectivity of the pores is

Table 4
Values of Eh and Ev at different confining pressures.

Confining pressure (MPa)	E_h (GPa)	E_v (GPa)
5	4.43	4
10	6.05	5.5
15	11.24	9

Table 5
Parameter values of the numerical model.

h_{p0}	ν_{vh}	ν_{hh}	φ_0 (°)	c_0 (MPa)	G_{vh} (GPa)	b_p
0.01	0.22	0.14	42.52	2.317	4.42	20

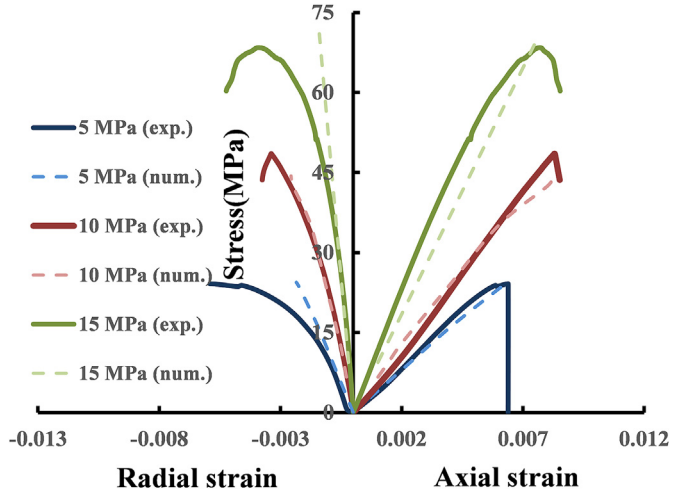

Fig. 10. Conventional triaxial test (exp.) results and simulations (num.).

poor. These characteristics may weaken the seepage effect during the radioactive waste geological disposal, which would be beneficial to the long-term stability of the repository.

In addition, the permeability of clayey rocks varies with the temperature. In the range of 20 °C–80 °C, the intrinsic permeability of Tamusu mudstone increases with increasing temperature, whereas those of Opalinus clay and COx argillite decrease with increasing temperature (Monfared et al., 2014; Zhang et al., 2017). The intrinsic permeability of Boom clay first slightly decreases with increasing temperature and subsequently remains constant (Ma et al., 2016). During cooling, the intrinsic permeability of Tamusu mudstone, Opalinus clay, and COx argillite decreases with decreasing temperature (Monfared et al., 2014; Zhang et al., 2017), whereas that of Boom clay first remains constant and subsequently slightly increases with decreasing temperature (Ma et al., 2016). Different trends of the intrinsic permeability of clayey rocks may be related to the sensitivity of structure to the temperature. Although the permeability of Tamusu mudstone increases in the heating stage, its highest value is about 4×10^{-20} m^2 (at 80 °C), which is still at a very low level. In general, the permeability of Tamusu mudstone is beneficial to prevent the spread of nuclides during the long-term operation of the HLW repository.

7. Conclusions

In this paper, the physico-mechanical properties of Tamusu mudstone are obtained by a series of experimental studies, including XRD, SEM, disintegration tests, permeability tests and conventional triaxial compression tests. The results show that

Table 6
Basic physico-mechanical parameters of candidate host clayey rocks for HLW repositories.

Rock	Density (g/cm^3)	Water content (%)	Intrinsic permeability (m^2)	Hydraulic conductivity (m/s)	Elastic modulus (GPa)	Poisson's ratio	Compressive strength (MPa)
Tamusu mudstone (this study)	2.55	2.2	1×10^{-20}	1×10^{-13}	4	0.3	24.1
Opalinus clay (Bossart et al., 2004)	2.45	6.6	2×10^{-20}	2×10^{-13}	2.8	0.23	25.6
COx argillite (Andra, 2005)	2.42	6.7	1×10^{-19}	1×10^{-12}	4.9	0.3	26
Boom clay (Chen et al., 2011)	1.9	27.5	3×10^{-19}	3×10^{-12}	0.7	0.125	2.2

Tamusu mudstone could be an ideal candidate host rock for HLW repositories. The main conclusions can be drawn as follows:

(1) Tamusu mudstone displays a high granular mineral content and closely arranged microstructure, which makes it maintain its physical properties when exposed to water and make it difficult to disintegrate. The clay minerals and analcite in Tamusu mudstone have strong ion exchange characteristics and adsorption capacity, which can effectively prevent radionuclide migration. Pyrite in Tamusu mudstone can reduce the high-valence radionuclides, reduce their migration and diffusion capacity, and consume the H_2O_2 produced by radiation.

(2) Tamusu mudstone displays a high density of 2.55 g/cm^3, an elastic modulus of 4 GPa in the direction perpendicular to the bedding plane, and a compressive strength of about 24 MPa, which is a kind of hard clayey rock. The SEM analysis shows that the microstructure of Tamusu mudstone is closely arranged, contains some microcracks and pores, and has obvious anisotropy. The mineral composition of Tamusu mudstone is primarily quartz, plagioclase, and dolomite, which are responsible for the high compressive strength, brittle failure, and other mechanical characteristics of the material.

(3) The permeability test shows that the hydraulic conductivity and intrinsic permeability of Tamusu mudstone are relatively low. Even when the temperature increases to 80 °C, the hydraulic conductivity of Tamusu mudstone is only 1×10^{-12} m/s. Moreover, its microstructural characteristics can well explain its low permeability. The low permeability can also effectively prevent radionuclide migration and diffusion and ensure the safety of the ecosystem outside the surrounding rock. The trends of the hydraulic conductivity and intrinsic permeability of Tamusu mudstone are in accordance with the temperature changes. Under the same temperature, the hydraulic conductivity and intrinsic permeability during cooling are larger than those during heating. This phenomenon indicates that the microstructure of Tamusu mudstone will irreversibly change when it is heated.

(4) Compared with Opalinus clay in Switzerland, COx argillite in France and Boom clay in Belgium, Tamusu mudstone shows itself advantages in terms of the geological disposal of HLW, which will be beneficial to the long-term safety and stability of the repository. Furthermore, analcime in Tamusu mudstone will enhance the radionuclide adsorption properties more than other clayey rocks. Future studies should focus on the mechanical properties, seepage flow, self-sealing characteristics and long-term rheological properties of Tamusu mudstone under THM coupling.

Declaration of competing interest

The authors declare that they have no known competing financial interests or personal relationships that could have appeared to influence the work reported in this paper.

Acknowledgments

The authors gratefully thank the general programs of the National Natural Science Foundation of China (Grant Nos. 51979266 and 51879258) and the Youth Innovation Promotion Association of the Chinese Academy of Sciences for their support of this study. The authors are also grateful to the editors and reviewers for their valuable comments, which have substantially improved this paper.

References

Amann, F., Button, E.A., Evans, K.F., Gischig, V.S., Blümel, M., 2011. Experimental study of the brittle behavior of clay shale in rapid unconfined compression. Rock Mech. Rock Eng. 44 (4), 415–430.
Amann, F., Kaiser, P., Button, E.A., 2012. Experimental study of brittle behavior of clay shale in rapid triaxial compression. Rock Mech. Rock Eng. 45 (1), 21–33.
Andra, 2005. Dossier2005: Andra Research on the Geological Disposal of High-Level Long-Lived Radioactive Waste: Result and Perspectives. French National Radioactive Waste Management Agency (Andra), Bure, France.
Armand, G., Bumbieler, F., Conil, N., de la Vaissière, R., Bosgiraud, J.M., Vu, M.N., 2017a. Main outcomes from in situ thermo-hydro-mechanical experiments programme to demonstrate feasibility of radioactive high-level waste disposal in the Callovo-Oxfordian claystone. J. Rock Mech. Geotech. Eng. 9 (3), 415–427.
Armand, G., Conil, N., Talandier, J., Seyedi, D.M., 2017b. Fundamental aspects of the hydromechanical behaviour of Callovo-Oxfordian claystone: from experimental studies to model calibration and validation. Comput. Geotech. 85, 277–286.
Bastiaens, W., Bernier, F., Li, X.L., 2006. An Overview of Long-Term HM Measurements Around HADES URF. Belgian Nuclear Research Centre (SCK·CEN), Mol, Belgium.
Bastiaens, W., Bernier, F., Li, X.L., 2007. SELFRAC: experiments and conclusions on fracturing, self-healing and self-sealing processes in clays. Phys. Chem. Earth 32 (8–14), 600–615.
Bieniawski, Z.T., Bernede, M.J., 1979. Suggested methods for determining the uniaxial compressive strength and deformability of rock materials 1: suggested method for determination of the uniaxial compressive strength of rock materials. Int. J. Rock Mech. Min. Sci. Geomech. Abstr. 16 (2), 138–140.
Bossart, P., Jaeggi, D., Nussbaum, C., 2017. Experiments on thermo-hydro- mechanical behaviour of Opalinus Clay at Mont Terri rock laboratory, Switzerland. J. Rock Mech. Geotech. Eng. 9 (3), 502–510.
Bossart, P., Trick, T., Meier, P.M., Mayor, J.C., 2004. Structural and hydrogeological characterisation of the excavation-disturbed zone in the Opalinus clay (Mont Terri project, Switzerland). Appl. Clay Sci. 26 (1–4), 429–448.
Boulin, P.F., Bretonnier, P., Gland, N., Lombard, J.M., 2012. Contribution of the steady state method to water permeability measurement in very low permeability porous media. Oil Gas Sci. Technol. 67 (3), 387–401.
Chen, G.J., Sillen, X., Verstricht, J., Li, X.L., 2011. ATLAS III in situ heating test in boom clay: field data, observation and interpretation. Comput. Geotech. 38 (5), 683–696.
Chen, T., Tian, W.Y., Li, C., Liu, X.Y., Wang, L.H., Sun, M., Zheng, Z., Zhu, J.B., Liu, C.L., 2010. Role of Pyrite in maintaining the reductive environment of the near field for a high-level radioactive waste repository. Acta Phys. Chim. Sin. 26 (9), 2489–2493.
Croise, J., Schlickenrieder, L., Marschall, P., Boisson, J.Y., Vogel, P., Yamamoto, S., 2004. Hydrogeological investigations in a low permeability claystone formation: the Mont Terri Rock Laboratory. Phys. Chem. Earth 29 (1), 3–15.
de la Vaissière, R., Armand, G., Talandier, J., 2015. Gas and water flow in an excavation-induced fracture network around an underground drift: a case study for a radioactive waste repository in clay rock. J. Hydrol. 521, 141–156.
De Bruyn, D., Thimus, J.F., 1996. The influence of temperature on mechanical characteristics of Boom clay: the results of an initial laboratory programme. Eng. Geol. 41 (1–4), 117–126.
Dehandschutter, B., Vandycke, S., Sintubin, M., Vandenberghe, N., Gaviglio, P., Sizun, J.P., Wouters, L., 2004. Microfabric of fractured Boom Clay at depth: a case study of brittle-ductile transitional clay behaviour. Appl. Clay Sci. 26 (1–4), 389–401.

Dehandschutter, B., Vandycke, S., Sintubin, M., Vandenberghe, N., Wouters, L., 2005. Brittle fractures and ductile shear bands in argillaceous sediments: inferences from Oligocene Boom Clay (Belgium). J. Struct. Geol. 27 (6), 1095–1112.
Delage, P., Sultan, N., Cui, Y.J., 2000. On the thermal consolidation of Boom clay. Can. Geotech. J. 37 (2), 343–354.
Du, J.J., Qin, X.G., Zeng, Q.L., Zhang, L.Q., Chen, Q., Zhou, J., Meng, W., 2017. Estimation of the present-day stress field using in-situ stress measurements in the Alxa area, Inner Mongolia for China's HLW disposal. Eng. Geol. 220, 76–84.
He, H.Y., Liu, J., Dong, Y., Li, H.H., Zhao, S.W., Wang, J., Jia, M.L., Zhang, H., Liao, J.L., Yang, J.J., Yang, Y.Y., Liu, N., 2019. Sorption of selenite on Tamusu clay in simulated groundwater with high salinity under aerobic/anaerobic conditions. J. Environ. Radioact. 203, 210–219.
Helmy, A.K., 1998. The limited swelling of montmorillonite. J. Colloid Interface Sci. 207 (1), 128–129.
Hensen, E.J.M., Smit, B., 2002. Why clays swell. J. Phys. Chem. B 106 (49), 12664–12667.
Homand, F., Giraud, A., Escoffier, S., Koriche, A., Hoxha, D., 2004. Permeability determination of a deep argillite in saturated and partially saturated conditions. Int. J. Heat Mass Tran. 47 (14–16), 3517–3531.
Hong, P.Y., Pereira, J.M., Cui, Y.J., Tang, A.M., Collin, F., Li, X.L., 2014. An elastoplastic model with combined isotropic-kinematic hardening to predict the cyclic behavior of stiff clays. Comput. Geotech. 62, 193–202.
Huang, H., 2018. Study on Hydrogeological Conditions of Clay Rock Pre-selected Section of High-Level Radioactive Waste Repository – Taking Tamusu and Suhongtu as Examples. MSc Thesis. East China University of Technology, Fuzhou, China (in Chinese).
Kong, L.W., Zeng, Z.X., Bai, W., Wang, M., 2018. Engineering geological properties of weathered swelling mudstones and their effects on the landslides occurrence in the Yanji section of the Jilin-Hunchun high-speed railway. Bull. Eng. Geol. Environ. 77 (4), 1491–1503.
Kull, H., Jockwer, N., Zhang, C.L., Wileveau, Y., Pepa, S., 2007. Measurement of thermally-induced pore-water pressure increase and gas migration in the Opalinus Clay at Mont Terri. Phys. Chem. Earth 32 (8–14), 937–946.
Ma, Y.S., Chen, W.Z., Gong, Z., Yu, H.D., Li, F.F., Li, X.L., 2018. Coupled thermo-hydro-mechanical anisotropy characteristics of clay based on the ATLAS III in situ heating test. Rock Soil Mech. 39 (2), 426–436 (in Chinese).
Ma, Y.S., Chen, W.Z., Yu, H.D., Gong, Z., Li, X.L., 2016. Variation of the hydraulic conductivity of Boom Clay under various thermal-hydro-mechanical conditions. Eng. Geol. 212, 35–43.
Martin, C.D., Lanyon, G.W., 2003. Measurement of in-situ stress in weak rocks at Mont Terri rock laboratory, Switzerland. Int. J. Rock Mech. Min. Sci. 40 (7–8), 1077–1088.
Monfared, M., Sulem, J., Delage, P., Mohajerani, M., 2014. Temperature and damage impact on the permeability of Opalinus Clay. Rock Mech. Rock Eng. 47 (1), 101–110.
Morrow, C.A., Moore, D.E., Lockner, D.A., 2000. The effect of mineral bond strength and adsorbed water on fault gouge frictional strength. Geophys. Res. Lett. 27 (6), 815–818.
Thury, M., Bossart, P., 1999. The Mont Terri rock laboratory, a new international research project in a Mesozoic shale formation. In: Switzerland. Eng. Geol., 52, pp. 347–359, 3–4.
Van Marcke, P., Bastiaens, W., 2010. Excavation induced fractures in a plastic clay formation: observations at the HADES URF. J. Struct. Geol. 32 (11), 1677–1684.
Wang, Y., Liang, H.A., Zhang, M.S., Yang, Z.P., 2017. Study on correlation between mineralogical composition and elastic modulus of clay rock for geological repository at home and abroad. Adv. Eng. Res. 135, 207–211.
Weetjens, E., Sillen, X., 2005. Thermal Analysis of the Supercontainer Concept. Belgian Nuclear Research Centre (SCK·CEN), Mol, Belgium.
Wersin, P., Van Loon, L.R., Soler, J.M., Yllera, A., Eikenberg, J., Gimmi, T., Hernan, P., Boisson, J.Y., 2004. Long-term diffusion experiment at Mont Terri: first results from field and laboratory data. Appl. Clay Sci. 26 (1–4), 123–135.
Wu, D.X., Liu, H.J., Wang, G.Q., 2010. Laboratory experimental study of slaking characteristics of red-bed soft rock. Chin. J. Rock Mech. Eng. 29 (Suppl. 2), 4173–4179.
Xiang, L., Liu, X.D., Liu, P.H., Jiang, X.F., Dai, C.C., 2020. Mineralogical and hydraulic characteristics of mudstone in the Tamusu candidate area in northwest China for high-level radioactive waste geological disposal. Clay Miner. 55 (1), 71–82.
Yang, D.S., Chen, W.Z., Wang, L.L., Chen, L.F., Wang, W., 2019. Experimental microscopic investigation of the cyclic swelling and shrinkage of a natural hard clay. Geotechnique 69 (6), 481–488.
Yu, H.D., Chen, W.Z., Gong, Z., Ma, Y.S., Chen, G.J., Li, X.L., 2018. Influence of temperature on the hydro-mechanical behavior of Boom Clay. Int. J. Rock Mech. Min. Sci. 108, 189–197.
Yu, H.D., Chen, W.Z., Gong, Z., Tan, X.J., Ma, Y.S., Li, X.L., Sillen, X., 2015. Creep behavior of boom clay. Int. J. Rock Mech. Min. Sci. 76, 256–264.
Yu, H.D., Chen, W.Z., Jia, S.P., Cao, J.J., Li, X.L., 2012. Experimental study on the hydro-mechanical behavior of Boom clay. Int. J. Rock Mech. Min. Sci. 53, 159–165.
Yu, H.D., Chen, W.Z., Li, X.L., Sillen, X., 2014. A transversely isotropic damage model for Boom Clay. Rock Mech. Rock Eng. 47 (1), 207–219.
Zhang, C.L., 2016. The stress–strain–permeability behaviour of clay rock during damage and recompaction. J. Rock Mech. Geotech. Eng. 8 (1), 16–26.
Zhang, C.L., 2018. Thermo-hydro-mechanical behavior of clay rock for deep geological disposal of high-level radioactive waste. J. Rock Mech. Geotech. Eng. 10 (5), 992–1008.
Zhang, C.L., Conil, N., Armand, G., 2017. Thermal effects on clay rocks for deep disposal of high-level radioactive waste. J. Rock Mech. Geotech. Eng. 9 (3), 463–478.
Zhang, H., Dong, Y., He, H.Y., Li, H.H., Zhao, S.W., Liu, J., Jia, M.L., Yang, J.J., Yang, Y.Y., Liu, N., Liao, J.L., 2020. Sorption of cesium on Tamusu clay in synthetic groundwater with high ionic strength. Radiochim. Acta 108 (4), 287–296.

Dr. Weizhong Chen is a professor at State Key Laboratory of Geomechanics and Geotechnical Engineering, Institute of Rock and Soil Mechanics, Chinese Academy of Sciences, China. His research interests cover rock mechanics and underground engineering. He is the author of 4 books and has published more than 200 scientific papers. He has won the Second Prize of National Science and Technology Progress Second Award, China.